Computational Condensed Matter 14 (2018) 15–19

Contents lists available at ScienceDirect

Computational Condensed Matter

journal homepage: www.elsevier.com/locate/cocom

Magnetic properties and electronic structure of $Bi_{0.75}Sm_{0.25}FeO_3$ multiferroic

A.F. Ravinski[a,*], I.I. Makoed[b], V.V. Triguk[b], V.V. Lazenka[c], A.I. Galyas[d], O.F. Demidenko[d], K.I. Yanushkevich[d], V.V. Moshchalkov[e]

[a] Bialystok University of Technology, Bialystok, Poland
[b] Brest State University Named After A.S. Pushkin, Brest, Belarus
[c] KU Leuven, Instituut voor Kernen Stralingsfysica, Celestijnenlaan 200 D, 3001 Leuven, Belgium
[d] Scientific-Practical Materials Research Center NASB, P.Brovki Str.19, Minsk, Belarus
[e] Institute for Nanoscale Physics and Chemistry, Celestijnenlaan Str., 200D, Leven, Belgium

ARTICLE INFO

Keywords:
Multiferroics
Magnetic spin structure
Electronic density functional method

ABSTRACT

Room temperature multiferroic $Bi_{0.75}Sm_{0.25}FeO_3$ samples were synthesized using a solid-state reaction method under high-pressure conditions (~4 GPA). The calculations of band structure, electronic and spin densities distribution of $Bi_{0.75}Sm_{0.25}FeO_3$ multiferroic were performed using the local spin-density approximation plus Hubbard U (LSDA + U) method in the framework of density functional theory. The calculations took into account a collinear antiferromagnetic ordering of the Fe and Sm magnetic moments. Temperature and field dependencies of the specific magnetization were investigated and correlated to the electronic structure of the multiferroic sample.

1. Introduction

Bismuth ferrite ($BiFeO_3$) based multiferroics with partial substitution of Bi^{3+} by rare earth elements are promising materials for developing new microelectronic devices due to the presence of the net magnetic moment and magnetoelectric interactions [1–4]. An unusual combination of the crystal ordering features and variation of the physical properties due to Sm substitution have already been observed in $Bi_{1-x}Sm_xFeO_3$ solid solution systems [5–7]. It has been shown in Ref. [5] that partial substitution of Bi cations by Sm (near 20 at.%) induced a polar rhombohedral to a nonpolar orthorhombic phase transition, which significantly enhanced magnetic performance of the sample. This means that full suppression of the spiral spin structure peculiar to pure $BiFeO_3$ [4] takes place due to the composition-driven transition from a rhombohedral to an orthorhombic phase. Additionally, improved dielectric and optical properties in the $Bi_{1-x}Sm_xFeO_3$ system have been demonstrated when Bi^{3+} was substituted by Sm^{3+} ions [7].

Mechanisms of the magnetic order formation and its structural dependences have not been clarified so far. That is why a theoretical investigation of the origin of the spin-ordered state in such multiferroic systems is of high importance. In this work, we present a study of magnetic properties and electronic structure of $Bi_{0.75}Sm_{0.25}FeO_3$ multiferroic based on experimental magnetization data and *ab-initio* calculations of band structure and spin density distribution of valence electrons.

2. Experimental details

The $Bi_{0.75}Sm_{0.25}FeO_3$ sample was synthesized by solid-state reaction method according to the ceramic technology [8] under 4 GPa pressure. The initial powders Bi_2O_3, Sm_2O_3, and Fe_2O_3 (chemical purity 99.99%, Sigma Aldrich Chemicals) were mixed manually. The stirring was performed for 0.5 h in a dry agate mortar and for 2 h with ethyl alcohol. The preliminary baking of the mixture was performed at a temperature of 850 ± 50 °C in a ceramic vessel in air for 3 h. The heating rate was 10 K/min. After grinding and final baking at the same conditions, X-ray diffraction and the final sintering by cold pressing at 4 GPa for 1 min were performed.

Studies on the chemical composition, performed using energy dispersive X-ray spectroscopy (EDX) in the scanning electron microscope (SEM) Hitachi S-3000N, confirm the chemical composition and purity.

The crystalline structure of the $Bi_{0.75}Sm_{0.25}FeO_3$ sample was characterized by X-ray diffraction (XRD) using DRON-3M diffractometer with CuK_α radiation. Rietveld refinements analysis with JANA2006 software [9] was used to determine the lattice parameters of the crystal.

Field dependencies of the specific magnetization were studied at

* Corresponding author.
E-mail addresses: a.ravinski@pb.edu.pl (A.F. Ravinski), igmak2010@yandex.ru (I.I. Makoed).

https://doi.org/10.1016/j.cocom.2017.11.006
Received 23 June 2017; Received in revised form 27 November 2017; Accepted 30 November 2017
Available online 05 December 2017

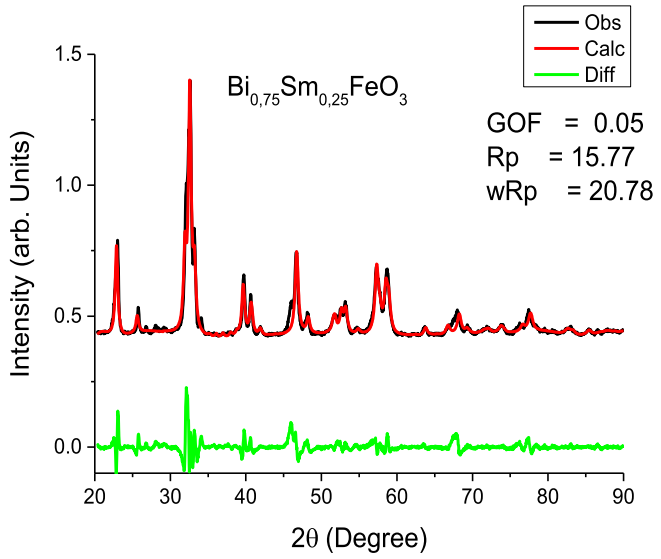

Fig. 1. Observed (black curve), calculated (red curve), and difference (lower green curve) XRD patterns for $Bi_{0.75}Sm_{0.25}FeO_3$ compound at room temperature. Fitting parameters Rp (residual of least-squares refinement), wRp (weighted residual) and GOF (goodness of fit) indicate very good refinement of a Rietveld model. (For interpretation of the references to colour in this figure legend, the reader is referred to the Web version of this article.)

temperatures 2 K, 10 K and 300 K in magnetic fields up to 5.5 T using SQUID magnetometry (Superconducting Quantum Interference Device, LOT-QuantumDesign MPMS-XL) and vibrating magnetometer (VSM, OXFORD). Temperature dependencies of the specific magnetization in the 2 to 80 K temperature range were measured using SQUID and 80 to 850 K by the ponderomotive (or Faraday's) method [10]. This method is based on the measurement of the mechanical force acting upon the specimen placed in a non-uniform magnetic field.

3. Crystal structure

The results of our XRD measurements and calculations are presented in Fig. 1. The XRD pattern was successfully fitted using the orthorhombic (space group Pbnm) model.

Table 1 presents equilibrium values of the Wyckoff positions, and lattice parameters determined experimentally and theoretically. The theoretical values of the lattice parameters were optimized by minimizing the total energy of the crystal E_{tot} as a function of the three lattice parameters a, b and c. Equilibrium lattice parameters are presented in Table 1. The data obtained in the work [11] is also presented in Table 1 for comparison. The $Bi_{0.75}Sm_{0.25}FeO_3$ crystal cell used in the calculation is shown in Fig. 2.

4. Magnetic charachterization

Magnetic field dependences of specific magnetization for the $Bi_{0.75}Sm_{0.25}FeO_3$ (Fig. 3) demonstrate the presence of a weak magnetic

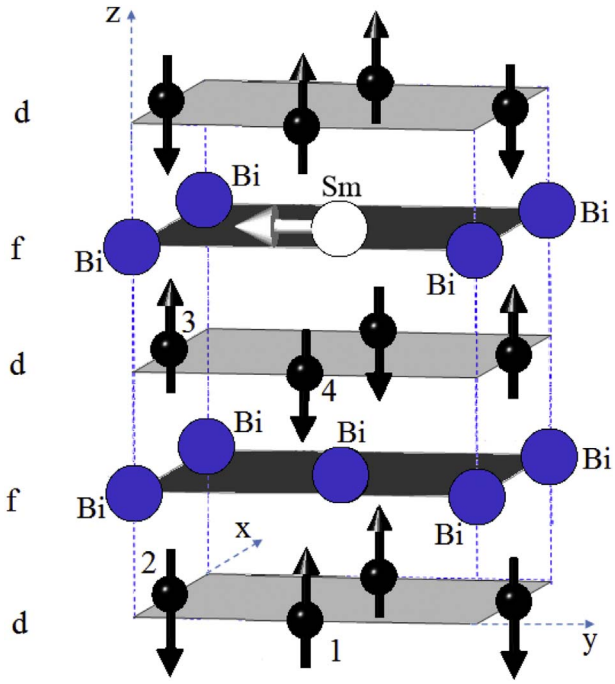

Fig. 2. Magnetic structure of the $Bi_{0.75}Sm_{0.25}FeO_3$. The black arrows indicate Fe^{3+} magnetic moments. The white arrow indicates the net magnetic moment of Sm^{3+} resulted from the spin canting along *x*-axis (see Fig. 6 below).

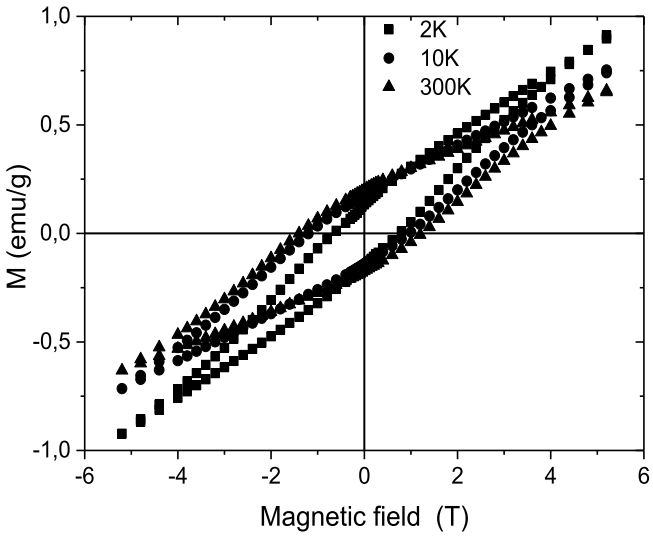

Fig. 3. Magnetic field dependence of the specific magnetization of the $Bi_{0.75}Sm_{0.25}FeO_3$ at 2 K, 10 K and 300 K.

Table 1
The equilibrium values of the Wyckoff positions and lattice parameters of the $Bi_{0.75}Sm_{0.25}FeO_3$ composition.

	x	y	z	Lattice parameters		
Bi^{3+}(75%) (4c)	0.5147	0.0555	0.2500	Theory	Experiment	Experiment [9]
Sm^{3+}(25%) (4c)	0.5147	0.0555	0.2500			
Fe^{3+} (4a)	0	0	0			
O_1^{2-} (4c)	0.4080	0.4740	0.2500			
O_2^{2-} (8d)	0.6970	0.8010	0.9550			
a, Å				5.3978	5.3936	5.1686
b, Å				5.5917	5.6001	5.0553
c, Å				7.7059	7.7645	7.4442

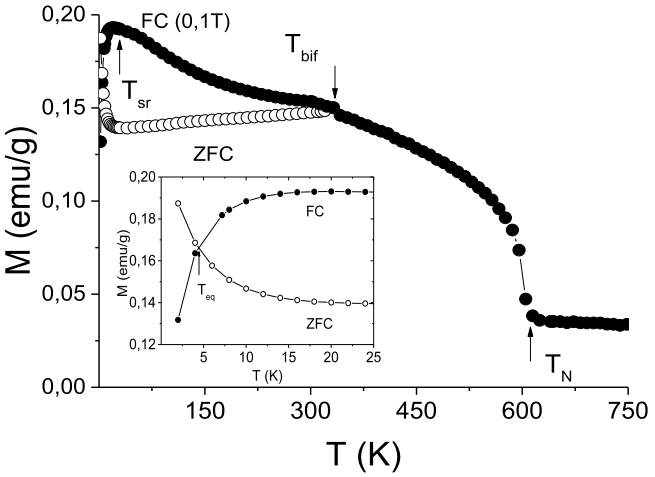

Fig. 4. Temperature dependence of the specific magnetization of the $Bi_{0.75}Sm_{0.25}FeO_3$.

moment in the sample. Substitution of Bi ions by Sm causes destruction of the long-range antiferromagnetic spin order intrinsic to $BiFeO_3$ and the appearance of the small net magnetic moment $(7{,}0–10{,}6) \cdot 10^{-3}$ μ_B. This changes the coercive field values in minor magnetic hysteresis loops and the remanence absolute values.

As seen in Fig. 4, the value of bifurcation temperature T_{bif}, where ZFC (zero field-cooled) and FC (field-cooled) magnetization temperature curves start to split, is 323 K. The spin-reorientation transition is observed at $T_{sr} \approx 21$ K. The presence of uncompensated magnetic moment is evident in the temperature range from 80 to 323 K. The absence of a pronounced maximum on the ZFC curve in the $T_{sr} < T < T_{bif}$ range confirms the presence of at least two mechanisms of magnetic ordering. The values of the specific magnetization, measured in ZFC and FC modes, are equal at a temperature of $T_{eq} = 4.4$ K. The Neel temperature is $T_N \approx 620$ K.

With increasing external magnetic field, the specific magnetization value increases and nearly reaches 1,0 Gauss·cm^3·g^{-1} at 5.5T, which corresponds to the magnetic moment value of $10.6 \cdot 10^{-3}$ μ_B. Magnetic properties of $Bi_{0.75}Sm_{0.25}FeO_3$ can be interpreted taking into account the presence of two magnetically active sublattices. Spin ordering in the samarium sublattice is sensitive to thermal motion of the atoms. The destruction of an antiferromagnetic order in the Sm^{3+} sublattice takes place at a temperature of 10 K [12]. The experimental results confirm the presence of two contributions at low temperatures: Sm^{3+} magnetic moments and a total magnetic moment arising due to the turn of the Fe^{3+} antiferromagnetically ordered moments. The received data indicate that the weak ferromagnetism in the $Bi_{0.75}Sm_{0.25}FeO_3$ at low temperatures is caused by the disruption of the collinearity of magnetic moments in both the *d*- and *f*-subsystems. For temperatures above 300 K, thermal motion destroys magnetic ordering of Sm^{3+} cations and a slight turn of the magnetic moments takes place only in the *d*-subsystem.

5. Band structure calculations

Band structure theoretical calculations were performed using electronic density functional method realized in the Wien-2k software complex [13]. Compounds with partially filled inner *d*- and *f*-shells are structures with a strongly correlated electronic subsystem. Therefore, to calculate exchange-correlation interaction, local spin-density approximation plus Hubbard U (LSDA + U) in the Kohn-Sham Hamiltonian was used [14]. The calculations were performed using the full-potential linear muffin-tin-orbital (FP-LMTO) method. The local exchange-correlation potential (Vxc) parametrized by Vosko et al. [15] was used. In the process of a self-consistent solution of the Kohn-Sham equations, 16 valence electrons for Sm ($4f^5 5s^2 5p^6 5d^1 s^2$), [8for Fe ($3d^6 4s^2$), 5 for Bi

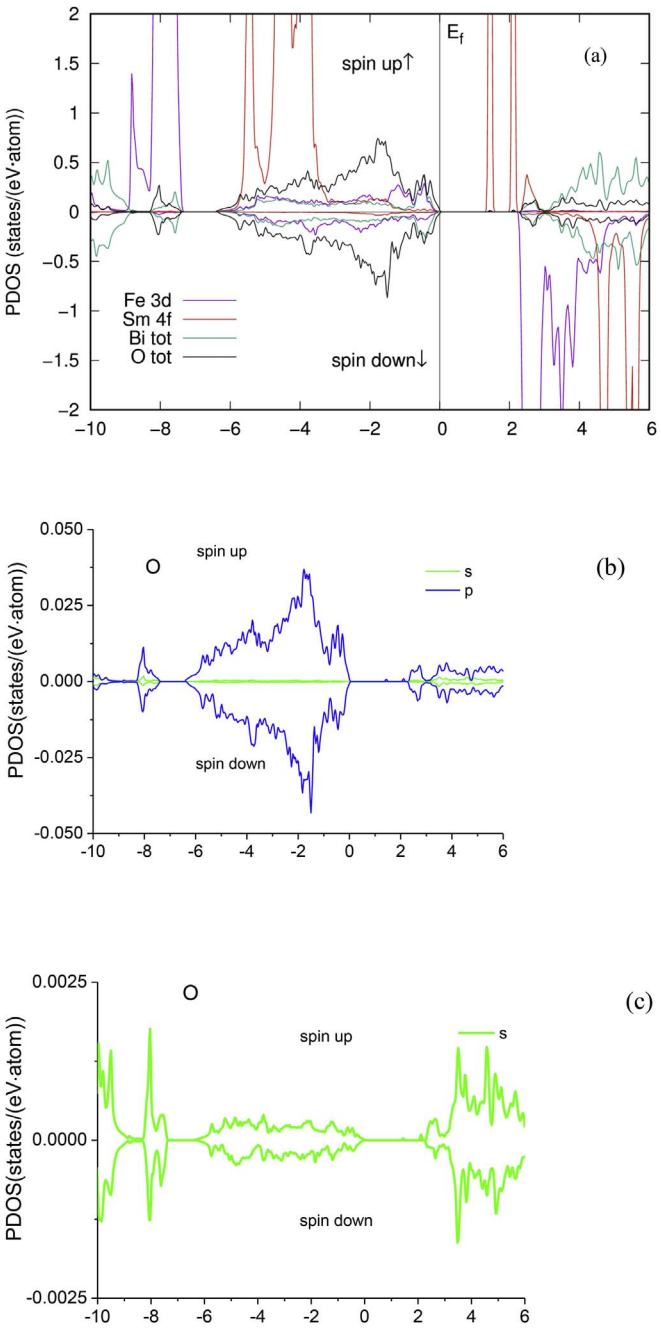

Fig. 5. (a) Total and partial electron density of states for Fe, Sm, Bi, O in the $Bi_{0.75}Sm_{0.25}FeO_3$; (b) Partial density of states for O and (c) Density of s-states for O.

($6s^2 6p^3$) and 6 for O ($2s^2 2p^4$) were taken into account. Integration over the Brillouin zone was performed according to the Monkhorst-Pack grid $5 \times 5 \times 5$ scheme (which corresponds to 8***k*** points in the irreducible wedge of the Brillouin zone in the orthorhombic symmetry) until the optimal values of the lattice parameters (corresponding to the values of Hellman-Feynman forces of 10^{-6} Ha/Bohr) were reached. The values of the muffin-tin radii were: 2.5 a.u. for Bi and Sm, 2.0 a.u. for Fe and 1.68 a.u. for O. The maximum kinetic energy of the plane waves was set to 25 Ha.

It was shown in Ref. [16] that theoretical values of the lattice parameters of the orthoferrites weakly depend on the magnetic symmetry type. These calculations took into account the spin polarization in the form of a homogeneous collinear antiferromagnetic (AFM) G-type ordering for the Fe^{3+} cations (*d*-subsystem) and C-type for the Sm^{3+} cations (*f*-subsystem) in accordance with the neutron diffraction

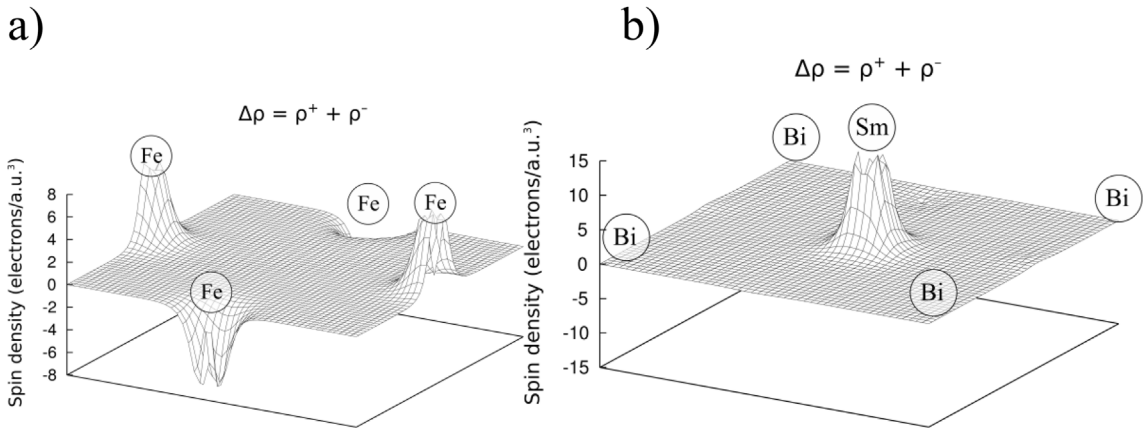

Fig. 6. Differential spin density maps of the valence electrons in the $Bi_{0.75}Sm_{0.25}FeO_3$ for magnetic (a) *d*- and (b) *f*-sublattices.

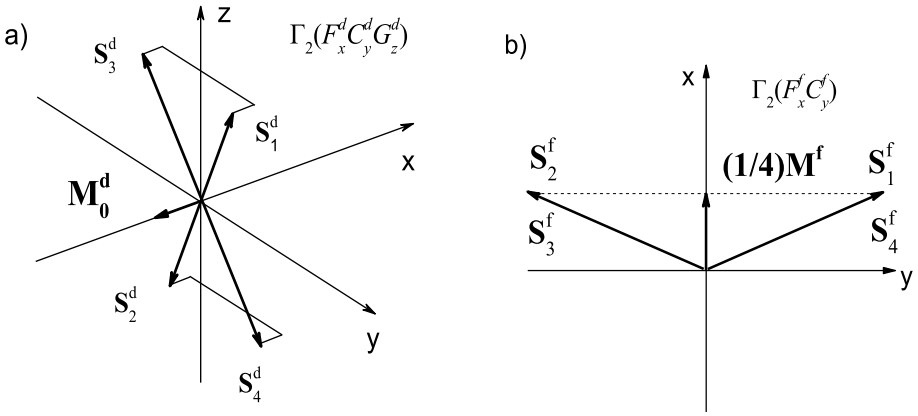

Fig. 7. Magnetic configuration of (a) *d*-sublattice and (b) *f*-sublattice of the $Bi_{0.75}Sm_{0.25}FeO_3$.

studies on orthoferrites isostructural samples [17,18]. Parameters of the correlation interaction were set: U_{eff} = 4 eV for *3d*-electrons of iron and U_{eff} = 6 eV for *4f* - and *5d*-electrons of samarium. The results showed that the stabilization of the electronic structure occurs at these U_{eff} values [19,20].

The calculated partial electronic densities of states for different spin directions for the valence electrons (spin up and spin down) are shown in Fig. 5.

The calculations show that the $Bi_{0.75}Sm_{0.25}FeO_3$ is a semiconductor with a band gap E_g of 1.28 eV. The conduction band is formed out mostly of the iron spin-down *3d*-states. Two peaks at 1,28 eV and 1,95 eV, related to the spin-up *4f*-states of samarium, act as a "filter" for electrons with a certain spin orientation of the magnetic moment. Energy levels of the strongly correlated iron *3d*-states and samarium *4f*-states are mostly located in the valence band with a positive (spin-up) spin direction. The bottom of the conduction band is formed out of the iron *3d*-states with a negative (spin-down) spin orientation and samarium *4f*-states with a positive (spin-up) spin direction. The top of the valence band is mainly presented by *2s*- and *2p*-states of the oxygen electrons. However, the contribution of *s* electrons is almost one order of magnitude lower than *p* electrons (see Fig. 5b and c). As seen in the electron density maps (Fig. 5a), there is a high valence electrons density of the O^{2-} ligands between the iron cations, which occupy *4c* and *8d* Wyckoff positions. The same situation occurs in the *f*-sublattice. The obtained results indicate the predominant role of the indirect exchange interactions Fe^{3+} - O^{2-} - Fe^{3+} and Sm^{3+} - O^{2-} - Sm^{3+} compared to the direct interactions Fe^{3+} - Fe^{3+}, Sm^{3+} - Sm^{3+}, Fe^{3+} - Sm^{3+}. The differential spin density distributions Δρ = ρ↑-ρ↓ (where ρ↑ and ρ↓ are the valence-electron spin density with spin-up and spin-down respectively) for the *d*- and *f*-sublattices are shown in Fig. 6. It is clear that the spin densities in the *d*- and *f*-sublattices are qualitatively different and form two magnetic subsystems. Interaction between these subsystems determines the magnetic characteristics of the material.

The theoretical foundations of the formation of magnetic structures in orthoferrites are now quite well developed [21–23]. The weak ferromagnetism is due to the disruption of the collinearity of the Fe^{3+} ($\mathbf{S_i^d}$) and Sm^{3+} ($\mathbf{S_i^f}$) spin magnetic moments (Fig. 7a and b) [22,24]. According to results of neutron diffraction studies [16,24,25], the magnetic structure of the *d*-sublattice at T < T_{SR} is characterized by $\Gamma^2(F_x^dC_y^dG_z^d)$ symmetry. A supercell with 80 magnetoactive ions, which includes four unit cells, corresponds to an extended magnetic cell containing 16 Fe^{3+} ions and 4 Sm^{3+} ions. With this spin configuration, 4 neighboring Fe^{3+} cations in the extended cell form a ferromagnetic ordering along the *x*-axis $\mathbf{M_o^d} = \mathbf{S_1^d} + \mathbf{S_2^d} + \mathbf{S_3^d} + \mathbf{S_4^d}$ (as shown in Fig. 7a) due to the rotation of the $\mathbf{S_1^d}$, $\mathbf{S_2^d}$, $\mathbf{S_3^d}$ and $\mathbf{S_4^d}$ magnetic moments. The net magnetic moment of the magnetic cell is $\mathbf{M^d} = 4\mathbf{M_o^d}$. According to the symmetry laws, the $\Gamma_2(F_x^dC_y^dG_z^d)$ representation for the *d*-sublattice is compatible with the $\Gamma_2(F_x^fC_y^f)$ representation for the *f*-sublattice [21]. Within the framework of the studied model of the magnetic structure, the net weak ferromagnetic moment of the *f*-sublattice at zero magnetic field $\mathbf{M^f} = \mathbf{S_1^f} + \mathbf{S_2^f} + \mathbf{S_3^f} + \mathbf{S_4^f}$ is directed along the *x*-axis, as shown in Fig. 7b.

As seen in the inset in Fig. 4, in the absence of an external magnetic field (ZFC) the magnetization increases when the temperature decreases. This is because a non-collinear AFM ordering of the *f*-subsystem provides a positive contribution to the net magnetization at T < T_{sr}. Cooling in the FC mode leads to the opposite effect: spin structure of the *f*-subsystem simultaneously interacts with both an external magnetic field and an internal field of exchange interaction of the *d*-subsystem, leading to a decrease in the net magnetization. At temperatures above T_{sr}, the AFM ordering of the magnetic Sm^{3+} cations moments is destroyed, and the *f*-sublattice turns into paramagnetic state. At

T < 10 K, an additional contribution due to the weak direct exchange interaction between $Sm^{3+} - O^{2-} - Sm^{3+}$ is formed. As a result, the AFM order of G-type is created. With increased temperature, this type of order is destroyed due to thermal motion and only remains in the *f*-sublattice as a result of the much stronger $Fe^{3+} - O^{2-} - Fe^{3+}$ superexchange [26]. Net value of the magnetization, determined by the expression $\mathbf{M} = \mathbf{M^d}–\mathbf{M^f}$, allows to explain the experimentally observed behavior of the temperature dependence of the magnetization using the two-sublattice model.

The results of the magnetization measurement confirm that formation of the weak ferromagnetic state in the $Bi_{0.75}Sm_{0.25}FeO_3$ at low temperatures may be due to magnetic moments interactions in the *d*- and *f*-sublattices. The coexistence and concurrence of contributions from these spin-ordered structures determine the shape and values of the magnetization temperature dependences. The Sm^{3+} ion is located in a magnetic environment formed by superposition of an external field and the magnetic exchange interaction field of the *d*-subsystem. One of the reasons for this complex magnetization behavior is the concurrence of FM and AFM contributions because of frustration of the magnetic exchange interactions between magnetoactive subsystems.

6. Conclusion

The results of *ab-initio* (LSDA + U approximation of the DFT method) calculations of the band structure allow us to confirm that the $Bi_{0.75}Sm_{0.25}FeO_3$ multiferroic is a semiconductor with a band gap of 1.28 eV in the ground state. The key role in the formation of the energy bands near the Fermi level belongs to strongly correlated *3d*-electron states of iron cations and to *f*-electronic states of samarium cations. Topography maps of electron density distribution indicate the presence of a pronounced asymmetry in the *f*-sublattice. This asymmetry helped us to explain experimentally observed features of the magnetization temperature behavior in the framework of the two-sublattice (*d*- and *f*-) magnetic structure model.

Acknowledgments

The work was performed in the framework of State Scientific Research Program 2016–2020 “Physical materials science, new materials and technology” (subprogramme “Material Science and technology of materials”, task No. 1.35). We kindly acknowledge the financial support from the Research Foundation Flanders (FWO), and the Concerted Research Action (GOA/14/007).

References

[1] G. Catalan, J.F. Scott, Physics and applications of bismuth ferrite, Adv. Mater. 21 (2009) 2463–2485.
[2] G.A. Smolenskii, I.E. Chupis, Ferroelectromagnets, Sov. Phys. Usp. 25 (7) (1982) 475–493.
[3] A.P. Pyatakov, A.K. Zvezdin, Magnetoelectric materials and multiferroics, Sov. Phys. Usp. 55 (2012) 557–581.
[4] I. Sosnowska, M. Loewenhaupt, W.I.F. David, R.M. Ibberson, Investigation of the unusual magnetic spiral arrangement in $BiFeO_3$, Physica B 180/181 (1992) 117–118.
[5] V.A. Khomchenko, J.A. Paixão, V.V. Shvartsman, A. Kholkin, Effect of Sm substitution on ferroelectric and magnetic properties of BiFeO3, Scripta Mater. 62 (2010) 238–241.
[6] E. Gil-González, A. Perejón, P.E. Sánchez-Jiménez, M.A. Hayward, J.M. Criado, M.J. Sayagués, L.A. Pérez-Maqueda, Characterization of mechanosynthesized $Bi_{1-x}Sm_xFeO_3$ samples unencumbered by secondary phases or compositional inhomogeneity, J. Alloys Compd. 711 (2017) 541–551.
[7] H. Singh, K.L. Yadav, Structural, dielectric, vibrational and magnetic properties of Sm doped $BiFeO_3$ multiferroic ceramics prepared by a rapid liquid phase sintering method, Ceram. Int. 41 (8) (2015) 9285–9295.
[8] I.I. Makoed, A.F. Ravinski, Specific features of the evolution of magnetic properties of bismuth ferrite modified with rare-earth element cations, Phys. Solid State 57 (9) (2015) 1787–1792.
[9] Petříček, et al., Crystallographic computing system JANA2006: general features, Z. Kristallogr. 229 (5) (2014) 345–352.
[10] A.F. Ravinski, I.I. Makoed, K. Kokoshkevich, K.I. Yanushkevich, A.I. Galyas, V.V. Triguk, Magnetic properties and electron density distribution of $La_xBi_{1-x}FeO_3$, Inorg. Mater. 43 (8) (2007) 860–865.
[11] X. Chen, Y. Wang, Y. Yang, G. Yuan, J. Yin, Z. Liu, Structure, ferroelectricity and piezoelectricity evolutions of $Bi_{1-x}Sm_xFeO_3$ at various temperatures, Solid State Commun. 152 (2012) 497–500.
[12] A.K. Zvezdin, V.M. Matveev, A.A. Mukhin, A.I. Popov, Rare-earth Ions in Magnetically Ordered Crystals, Nauka, Moscow (1985) [in Russian]. 296 c.
[13] P. Blaha, K. Schwarz, G.K.H. Madsen, D. Kvasnicka, J. Luitz, K. Schwarz (Ed.), WIEN2K: Full Potential Linearized Augmented Plane Waves and Local Orbital Programs for Calculating Crystal Properties, Vienna University of Technology, Austria, 2001.
[14] S.L. Dudarev, L.-M. Peng, S.Y. Savrasov, J.-M. Zuo, Correlation effects in the ground-state charge density of Mott insulating NiO: a comparison of ab initio calculations and high-energy electron diffraction measurements, Phys. Rev. B 61 (2000) 2506–2512.
[15] S.H. Vosko, L. Wilk, M. Nusair, Can. J. Phys. 58 (8) (1980) 1200–1211.
[16] I.R. Shein, K.I. Shein, V.L. Kozhevnikov, A.L. Ivanovskii, Band structure and the magnetic and elastic properties of $SrFeO_3$ and $LaFeO_3$ perovskites, Phys. Solid State 47 (11) (2005) 2082–2088.
[17] S. Maruyama, et al., Change in the magnetic structure of (Bi,Sm)FeO_3 thin films at the morphotropic phase boundary probed by neutron diffraction, APL Mater. 2 (2014) 116106.
[18] W. Sławinski, R. Przeniosło, I. Sosnowska, E. Suard, Spin reorientation and structural changes in $NdFeO_3$, J. Phys. Cond. Matter 17 (2005) 4605–4614.
[19] A.F. Ravinski, V.V. Triguk, I.I. Makoed, Ab Initio calculations of the lattice dynamics and the ferroelectric instability of the $BiFeO_3$ multiferroic, Phys. Solid State 56 (9) (2014) 1799–1805.
[20] L. Chen, T. Li, S. Cao, S. Yuan, F. Hong, J. Zhang, The role of 4f-electron on spin reorientation transition of $NdFeO_3$: a first principle study, J. Appl. Phys. 111 (2012) 103905–1 – 103905-6.
[21] R.L. White, Review of recent work on the magnetic and spectroscopic properties of the rare earth orthoferrites, J. Appl. Phys. 40 (3) (1969) 1061–1069.
[22] T. Yamaguchi, K. Tsushima, Magnetic symmetry of rare-earth orthochromites and orthoferrites, Phys. Rev. B 8 (11) (1973) 5187–5198.
[23] A.K. Zvezdin, A.A. Mukhin, Magnetoelectric interactions and phase transitions in a new class of multiferroics with improper electric polarization, JETP Lett. 88 (8) (2008) 505–510.
[24] Y.K. Jeong, J.-H. Lee, S.-J. Ahn, H.M. Jang, Temperature-induced magnetization reversal and ultra-fast magnetic switch at low field in $SmFeO_3$, Sol. St. Commun. 152 (2012) 1112–1115.
[25] J.-H. Lee, Y.K. Jeong, J.H. Park, M.-A. Oak, H.M. Jang, J.Y. Son, J.F. Scott, Spin-canting-induced improper ferroelectricity and spontaneous magnetization reversal in $SmFeO_3$, Phys. Rev. Lett. 107 (2011) 117201–1-117201-5.
[26] A. Bombik, B. Lesniewska, J. Mayer, A.W. Pacyna, Crystal structure of solid solutions $REFe_{1-x}(Al \text{ or } Ga)_xO_3$ (RE = Tb, Er, Tm) and the correlation between superexchange interaction Fe^{+3} - O^{-2} - Fe^{+3} linkage angles and Neel temperature, J. Magn. Magn. Mater. 257 (2003) 206–219.